



HAL
open science

Understanding the nanoscale adhesion forces between the fungal pathogen *Candida albicans* and antimicrobial zinc-based layered double hydroxides using single-cell and single-particle force spectroscopies

Jazia Awassa, Samantha Soulé, Damien Cornu, Christian Ruby, Sofiane El-Kirat-Chatel

► To cite this version:

Jazia Awassa, Samantha Soulé, Damien Cornu, Christian Ruby, Sofiane El-Kirat-Chatel. Understanding the nanoscale adhesion forces between the fungal pathogen *Candida albicans* and antimicrobial zinc-based layered double hydroxides using single-cell and single-particle force spectroscopies. *Nanoscale*, 2024, 5 (3), pp.1171-1184. 10.1039/D3NR06027F . hal-04443296

HAL Id: hal-04443296

<https://hal.univ-lorraine.fr/hal-04443296>

Submitted on 7 Feb 2024

HAL is a multi-disciplinary open access archive for the deposit and dissemination of scientific research documents, whether they are published or not. The documents may come from teaching and research institutions in France or abroad, or from public or private research centers.

L'archive ouverte pluridisciplinaire **HAL**, est destinée au dépôt et à la diffusion de documents scientifiques de niveau recherche, publiés ou non, émanant des établissements d'enseignement et de recherche français ou étrangers, des laboratoires publics ou privés.



Distributed under a Creative Commons Attribution - NonCommercial 4.0 International License

1
2 Understanding the nanoscale adhesion forces
3 between the fungal pathogen *Candida albicans* and
4 antimicrobial zinc-based layered double hydroxides
5 using single-cell and single-particle force
6 spectroscopies

7 Jazia Awassa,¹ Samantha Soulé,¹ Damien Cornu,¹ Christian Ruby,¹ Sofiane El-Kirat-Chatel^{1,2*}

8 ¹Université de Lorraine, CNRS, LCPME, F-54000 Nancy, France

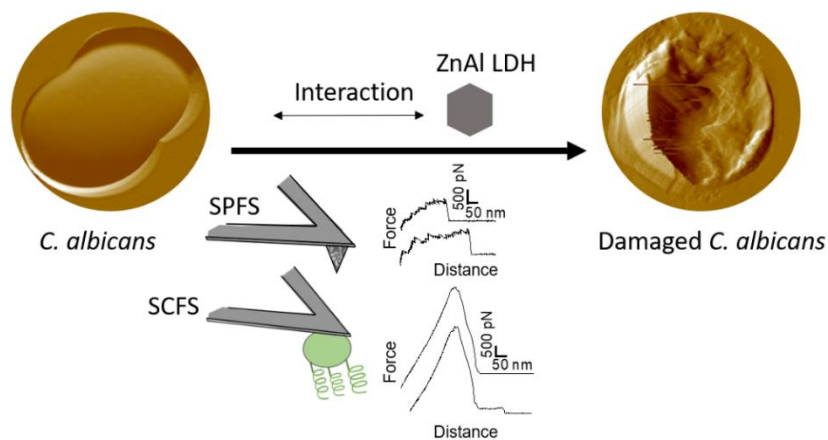
9 ²Univ. Bordeaux, CNRS, Bordeaux INP, CBMN, UMR 5248, F-33600 Pessac, France

10 *Corresponding author: Sofiane El-Kirat-Chatel: sofiane.elkirat@u-bordeaux.fr

11 **Abstract**

12 Antifungal resistance has become a major serious concern, and *Candida albicans* is considered as
13 one of the most opportunistic fungal pathogens responsible for several human infections. In this
14 context, the use of new antifungal agents such as zinc-based layered double hydroxides to fight
15 such fungal pathogens is considered as one possible mean to help limit the problem of antifungal
16 resistance. In this study, we show that ZnAl LDH nanoparticles exhibit remarkable antifungal

17 properties against *C. albicans* and cause serious cell wall damages as revealed by growth test and
18 atomic force microscopy (AFM) imaging. To further link the antifungal activity of ZnAl LDHs to
19 their adhesive behaviors toward *C. albicans* cells, AFM-based single-cell, and single-particle
20 force spectroscopies were used to probe the nanoscale adhesive interactions. The force
21 spectroscopy analysis revealed that antimicrobial ZnAl LDHs possess specific surface interactions
22 with *C. albicans* cells with remarkable force magnitudes and adhesion frequencies in comparison
23 to non-antifungal negative controls, e.g., Al-coated substrates and MgAl LDHs, which showed
24 limited interactions with *C. albicans* cells. Force signatures suggest that such adhesive interactions
25 may be attributed to the presence of Agglutinin-like sequence (Als) adhesive proteins at the cell
26 wall surface of *C. albicans* cells. Our findings propose the presence of a strong correlation between
27 the antifungal effect provided by ZnAl LDHs and their nanoscale adhesive interactions with *C.*
28 *albicans* cells at both the single-cell and single-particle levels. Therefore, ZnAl LDHs could
29 interact with *C. albicans* fungal pathogens by specific adhesive interactions through which they
30 adhere to fungal membranes, leading to their damage and subsequent growth inhibition.



31
32 ZnAl LDH NPs showed remarkable antifungal properties against *C. albicans* fungal cells. The
33 antifungal activity was linked to the adhesive specific interactions between ZnAl nanoparticles
34 and *C. albicans* which were probed by both SPFS and SCFS.

- 35 **Keywords**
- 36 Zinc-based LDH
- 37 Antibacterial activity
- 38 Direct contact mechanism
- 39 Atomic force microscopy
- 40 Single-particle force spectroscopy
- 41 Single-cell force spectroscopy

42 **1. Introduction**

43 Fungal infections lead to various human diseases, ranging from superficial cutaneous to serious
44 invasive fungal diseases (IFDs), which together are estimated to affect more than a billion people
45 worldwide.^{1,2} The number of antifungal agents used in clinics is very limited compared to that of
46 antibiotics.³ Historically, fungal infections treatment relied on four classes of clinical antifungal
47 drugs: polyenes, azoles, echinocandins and the pyrimidine analog 5-flucytosine.⁴ However, the
48 incidence of invasive fungal infections has been always on the rise and the problem of antifungal
49 resistance has become an emerging concern.^{5,6} For example, *Candida albicans* is a major
50 opportunistic fungal pathogen responsible for several human infections in different body parts such
51 as the oral cavity, skin, bloodstream, gastrointestinal tract, and vagina.⁷ Infections by *C. albicans*
52 could further lead to severe morbidity and mortality, especially in immunocompromised patients.⁸
53 Given the significant concern of fungal infections and the limited arsenal of existing antifungal
54 drugs, inorganic-based nanomaterials were considered as good candidates for developing new
55 antifungal agents.^{6,9} In this aspect, the use of pristine layered double hydroxides (LDHs) as
56 inorganic antifungal agents could play a very significant role. LDHs are anionic clays comprising
57 a structure based on the stacking of brucite-like sheets of divalent and trivalent metal hydroxides.
58 The net positive charge of these sheets is compensated by the presence of negatively charged
59 intercalating anions and water molecules in the interlaminar region.¹⁰⁻¹²

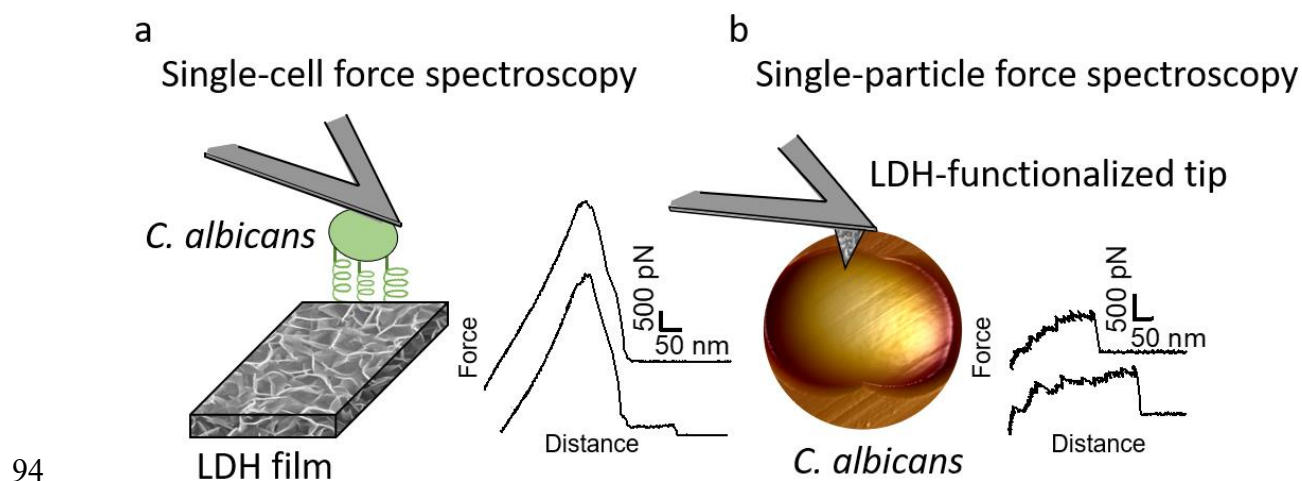
60 Several recent studies have shown that zinc-based pristine LDHs could act as efficient antibacterial
61 agents against various Gram-positive and Gram-negative bacterial strains.¹³⁻²⁰ Up to our
62 knowledge, the only study claiming the antifungal activity of LDHs against fungal pathogens is
63 that of Moaty *et al.*,¹³ by which the antibacterial and antifungal activity of ZnFe LDHs was tested
64 against broad range of bacterial and fungal pathogens. However, the authors admitted the

65 antifungal mechanism of LDHs was far from being understood, and therefore real experimental
66 setups explaining the antifungal effect of LDHs are still lacking.

67 One possible explanation of the antifungal activity of zinc-based LDHs is direct surface
68 interactions between the LDH surface and the cell wall of yeast cells. In our recent previous work,
69 we have determined the importance of the direct surface interactions mechanism between the
70 Gram-positive bacteria *Staphylococcus aureus* and ZnAl LDH nanoparticles (NPs) to their
71 antibacterial mode of action.¹⁴ Here, our interest was to determine whether ZnAl LDH NPs could
72 interact with *C. albicans* fungal pathogens to provide an efficient antifungal effect. Recently,
73 remarkable advances were employed in the use of atomic force microscopy (AFM)-based single-
74 cell and single-particle force spectroscopy (SCFS and SPFS, respectively) to probe the forces
75 driving cell–cell and cell–solid interactions.^{21–26} Yet, the methods were rarely implemented to
76 study the interactions between fungal pathogens and antifungal agents, *e.g.*, ZnAl LDHs. In fact,
77 SCFS and SPFS are powerful tools for probing the forces that drive cell–surface interactions.^{26,27}
78 The general principle of SCFS is to immobilize a single living cell on AFM tips and to record
79 force–distance curves between the cell probe and a substrate. Whereas SPFS mainly relies on
80 functionalizing AFM probes with particles/molecules to probe interactions with cells at the single
81 particle/molecule level.

82 In this work, the antifungal activity of ZnAl LDH NPs is evaluated against the fungal pathogen *C.*
83 *albicans* using agar disc diffusion assay and broth microdilution test to determine their minimum
84 inhibitory concentration (MIC). AFM imaging is employed to show the damage imposed by ZnAl
85 LDH NPs on the cell wall of *C. albicans* cells. *C. albicans* cells were further attached to AFM
86 tipless cantilevers to probe the nanoscale adhesion forces between these pathogenic yeasts and
87 ZnAl LDHs using SCFS (**Fig. 1a**). Moreover, we took advantage of our original approach to

88 functionalize AFM tips with LDH films to probe their interactions at the single-particle level using
89 AFM-based SPFS (**Fig. 1b**). Compared to the negative controls, *e.g.*, Al-coated surfaces and MgAl
90 LDH films, ZnAl LDHs possessed specific adhesion forces with the cell wall of *C. albicans* at
91 both the single-particle and single-cell levels. Such findings strongly support the correlation
92 between the efficient antifungal effect of ZnAl LDH NPs and their interactions with *C. albicans*
93 cells mediated by Als proteins adhesion molecules.

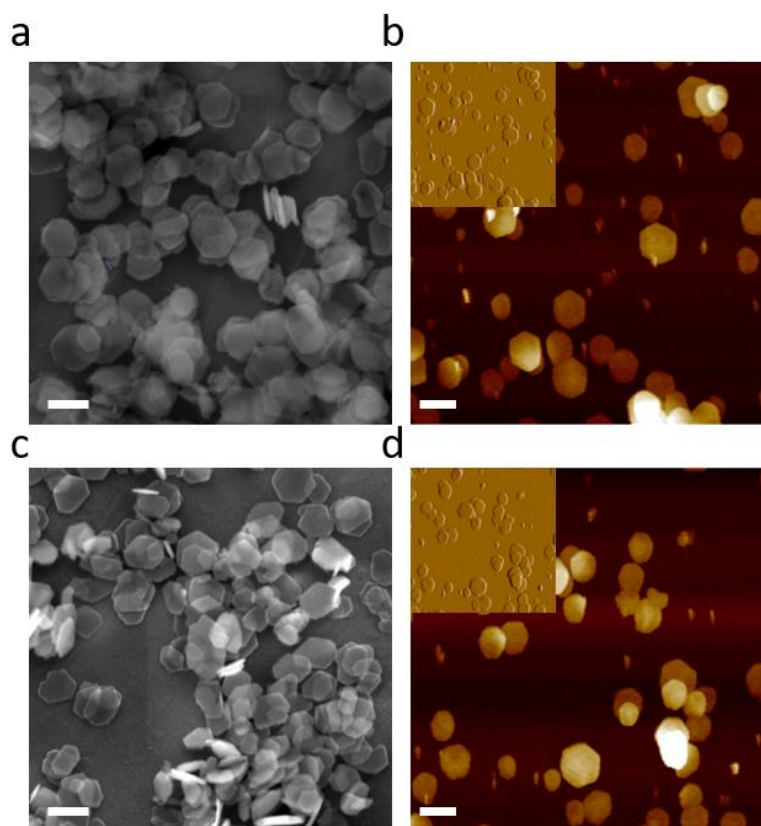


95 **Fig. 1.** Single-cell and single-particle force spectroscopy analysis of the interactions between ZnAl LDHs
96 and *C. albicans* cells. (a) For single-cell force spectroscopy, living *C. albicans* cells were attached to
97 polydopamine-coated tipless cantilevers. The adhesion forces between an individual yeast cell and a LDH
98 film grown on a silicon substrate were probed. On the right is an example of recorded force-distance curves.
99 (b) For single-particle force spectroscopy, LDH films were grown on the surface of silicon nitride AFM
100 tips. The adhesion forces between LDH particles and *C. albicans* cells immobilized on porous membranes
101 were probed. On the right is an example of recorded force-distance curves.

102 2. Results and discussion

103 2.1. ZnAl LDH NPs exhibit significant antifungal activity against *C. albicans*

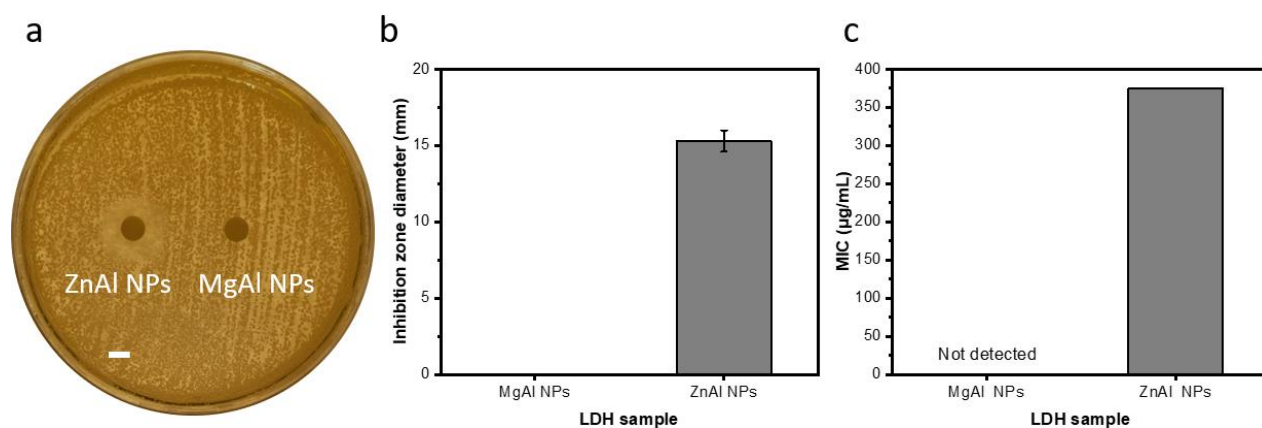
104 Before testing the antifungal activity of LDH NPs, ZnAl LDH NPs were prepared by a fast
105 coprecipitation method. MgAl LDH NPs were also prepared using a similar synthesis method
106 to serve as a negative control.



107
 108 **Fig. 2.** LDH NPs morphology. (a,c) SEM images of MgAl (a) and ZnAl (c) LDH NPs (scale bars = 200
 109 nm). (b,d) AFM height images of MgAl (b) and ZnAl (d) LDH NPs (scale bars = 200 nm, insets are
 110 corresponding deflection images showing the NPs surface ultra-structure).

111 Nitrate-intercalated MgAl and ZnAl LDH NPs having a $Zn^{II}:Al^{III}$ molar ratio of ~ 2 were prepared
 112 by the coprecipitation-hydrothermal method.¹⁴ Both LDH NPs presented a hexagonal lamellar
 113 structure as revealed by the SEM and AFM images (**Fig. 2**). The NPs also exhibited similar average
 114 particle sizes extracted by SEM imaging (169 ± 18 nm and 167 ± 40 nm, for MgAl and ZnAl NPs,
 115 respectively). Similar average particle sizes were also obtained from the AFM height images (170
 116 ± 30 nm and 167 ± 33 nm, for MgAl and ZnAl LDH NPs, respectively). Both LDH NPs were well
 117 crystallized presenting no crystalline, nor amorphous impurities as suggested by our previously
 118 performed XRD, XPS, and IR analysis.¹⁴ The detailed structural and morphological
 119 characterizations of these LDH NPs could be found in our recent previous study.¹⁴

120 The antifungal activity of MgAl and ZnAl LDH NPs was then tested against the fungal pathogen
121 *C. albicans* using the agar disk diffusion method. The generated inhibition zone diameters and
122 their mean values obtained from three repetitive experiments are presented in **Fig. 3**. Moreover,
123 the minimum inhibitory concentration (MIC) required to inhibit the growth of *C. albicans* by the
124 two LDH NPs was determined by broth microdilution turbidimetric tests performed for three
125 repetitive trials as well (**Fig. 3**).



126 **Fig. 3.** NPs antifungal activity against *C. albicans*. (a) Agar disk diffusion test using 10 mg/mL ZnAl and
127 MgAl NPs suspensions (scale bar = 5 mm). (b) Mean zone of inhibition of ZnAl and MgAl calculated as
128 the average inhibition diameters of three repetitive trials, and error bars represent the standard deviation of
129 the three obtained inhibition zone diameters. (c) MIC values for MgAl and ZnAl NPs determined from
130 three repetitive trials.

132 MgAl LDH NPs did not provide any antifungal effect revealed by any of the two antifungal activity
133 tests, and thus played the role of negative control. On the other hand, ZnAl LDH NPs showed
134 efficient antifungal activity against *C. albicans* with an average inhibition zone diameter of 15.3
135 mm and MIC value of 375 µg/mL. The antifungal activity against *C. albicans* fungal pathogen was
136 weaker than the antibacterial effect achieved by ZnAl LDH NPs against *S. aureus* (inhibition zone
137 diameter of 20.6 mm and MIC value of 93.8 µg/mL).¹⁴ Such difference between the antifungal and
138 antibacterial activity of ZnAl LDH NPs may be explained by the different tested microorganisms,
139 e.g., *C. albicans* and *S. aureus* cells, where each type of microorganism responds differently to the

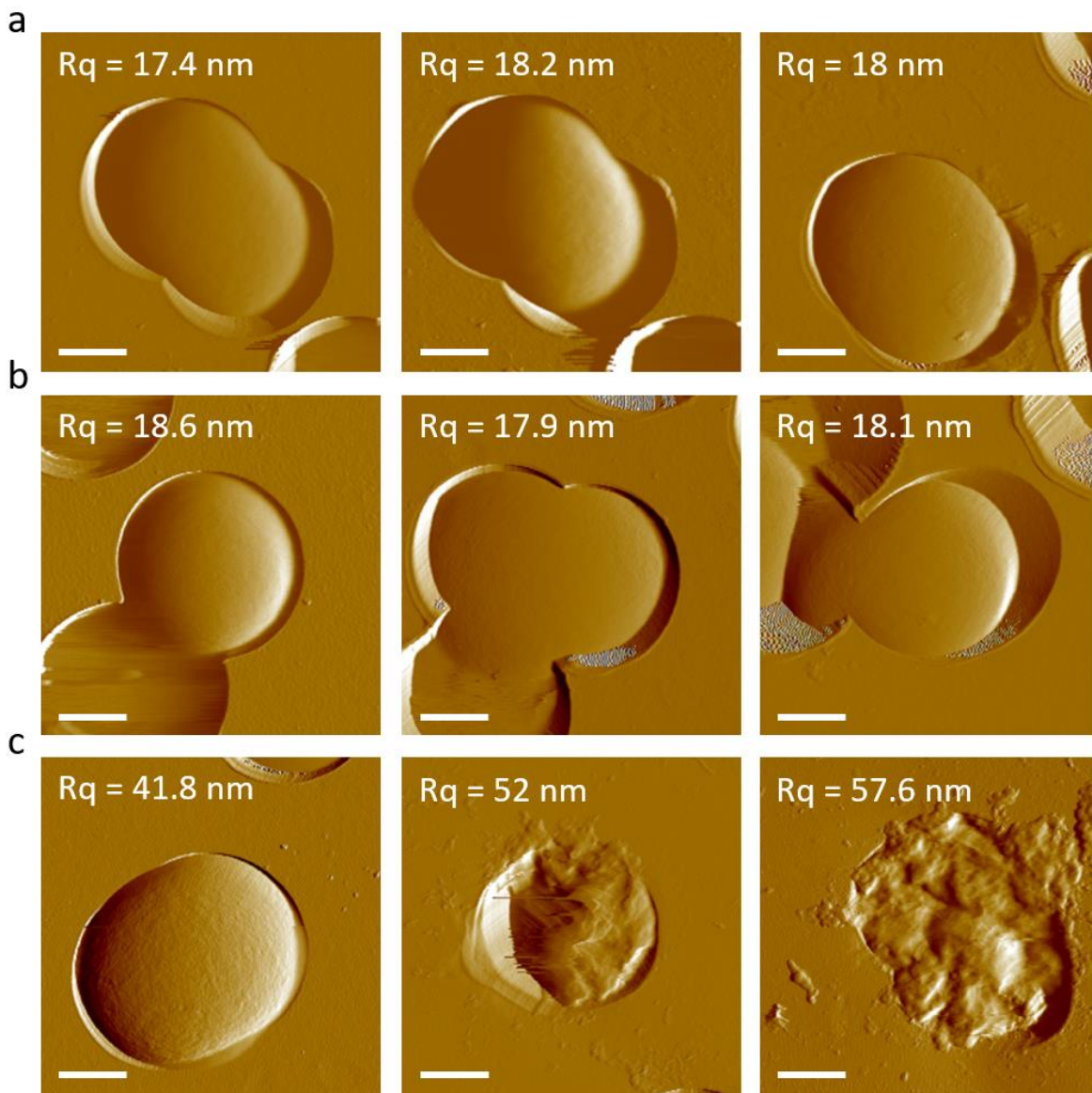
140 same biocide.^{13,28,29} Similarly, the antifungal activity of our ZnAl LDH NPs against *C. albicans*
141 fungal pathogens was weaker than that of ZnO NPs synthesized by Yassin *et al.* (inhibition zone
142 diameter = 24.18 mm and MIC value of 10 µg/mL),³⁰ but still greater than the antifungal activity
143 achieved by MgO and SiO₂ NPs prepared by Karimiyan *et al.* (MIC > 3200 µg/mL).³¹ Moreover,
144 Jalal *et al.* also reported a weaker antifungal activity of ZnO NPs against the same fungal strain
145 which showed a MIC value of 250 µg/mL.³² The difference in the antifungal activity with our
146 ZnAl LDH NPs, in this case, is attributed to the nature of the antifungal agent, or to the different
147 followed protocols used to perform the antifungal activity tests.^{15,16}

148 Compared to MgAl LDH NPs, the superior antifungal activity of ZnAl NPs could be attributed to
149 the nature of their constituent divalent metal, *e.g.*, Zn²⁺. We have previously shown that the
150 antimicrobial activity of pristine LDHs is strongly dependent on the nature of constituent divalent
151 metal,^{14,15} and it was previously reported that zinc-based LDHs have remarkable antibacterial
152 properties towards a broad range of bacteria.¹³⁻²⁰ Moreover, Moaty *et al.* who performed the only
153 antifungal study of ZnFe LDHs also claimed that the antifungal effect of the tested LDH sample
154 was attributed to the antifungal nature of the constituent zinc divalent metal.¹³ The antimicrobial
155 properties of zinc-based LDHs are generally attributed to their ability to adhere to microorganisms
156 and change their charge distribution, thus blocking the transport of nutrients in and out of the
157 membrane, or else by binding to the intracellular DNA leading to their denaturation.^{20,33,34} Such
158 antimicrobial action mode requires the presence of direct surface interactions between the LDH
159 surface and tested microorganisms, here *C. albicans*.

160 **2.2. ZnAl LDH NPs impose serious cell wall damage to *C. albicans* cells**

161 AFM imaging was used to visualize the surface topography of *C. albicans* cells before and
162 after treatment with MgAl and ZnAl LDH NPs at a concentration of 375 µg/mL, corresponding

163 to the MIC value of ZnAl LDH NPs. Additionally, the roughness parameter Rq (root mean
164 square of the heights) was obtained from AFM images performed on the top of yeast cells at a
165 high magnification of $1 \times 1 \mu\text{m}^2$ scanning areas.



166
167 **Fig. 4.** AFM deflection images of *C. albicans* cells in liquid (scale bar = $1 \mu\text{m}$). (a) Untreated *C. albicans*
168 cells. (b) *C. albicans* cells treated with MgAl LDH NPs at $375 \mu\text{g}/\text{mL}$ corresponding to the MIC value of
169 ZnAl LDH NPs. (c) *C. albicans* cells treated with ZnAl LDH NPs at $375 \mu\text{g}/\text{mL}$ corresponding to the MIC
170 value of ZnAl LDH NPs.

171 As shown in **Fig. 4a** and **b**, untreated yeast cells as well as those treated with non-antimicrobial
172 MgAl LDH NPs presented well-defined, intact shapes with smooth surfaces ($R_q = 17.9 \pm 0.5$ nm,
173 18.2 ± 0.4 nm, for untreated and MgAl NPs-treated cells, respectively).

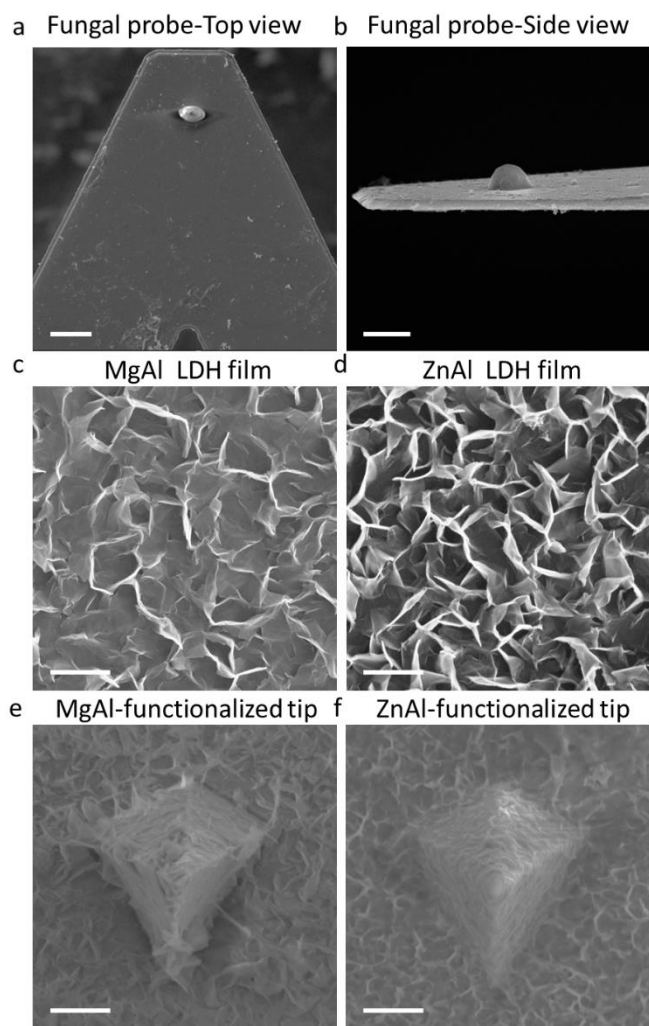
174 On the other hand, cells treated with antimicrobial ZnAl LDH NPs were distorted with highly
175 corrugated surfaces presenting hollows and crests (**Fig. 4c**). Similar cells damage observations
176 were previously reported on *C. albicans* cells treated with different biocides in air and liquid
177 conditions.³⁵⁻³⁸ Moreover, some cells were even completely damaged presenting irregular
178 morphologies, and dissociated cell walls leaving behind some cell debris within the polycarbonate
179 membrane pores. Additionally, cells treated with ZnAl LDH NPs were found to have ~2.5 times
180 rougher surfaces ($R_q = 50.4 \pm 8.6$ nm) than untreated and MgAl LDH NPs treated ones. The
181 increase in surface roughness of yeast cells suggests the existence of serious cell wall damage
182 induced by ZnAl LDH NPs. The structural integrity of the cell wall of *C. albicans* is an essential
183 element for its survival. Therefore, damages in the cell wall might cause osmotic disorders in the
184 fungal cell, rupture of the cell membrane, and subsequently the outflow of cellular and cytoplasmic
185 components leading to cell death.^{39,40}

186 All these observations suggest that ZnAl LDH NPs induce an efficient antifungal effect on *C.*
187 *albicans* cells by targeting their cell wall leading to their distortion, damage, and subsequently to
188 the death of the microorganism.

189 **2.3. Nanoscale adhesion forces between *C. albicans* and ZnAl LDHs**

190 To determine whether the antifungal activity of ZnAl LDHs is related to their ability to interact
191 with yeast cells leading to their damage, the nanoscale adhesion forces between *C. albicans*
192 and ZnAl LDHs were probed at the single-cell level. For this purpose, living *C. albicans* cells

193 were attached to tipless cantilevers coated with polydopamine acting as a bio-adhesive (**Fig.**
194 **5a and b**).^{21,26,27,41,42} The obtained fungal cell probes were brought into contact with ZnAl LDH
195 films grown on silicon substrates using a wet-chemistry adapted from Zhang *et al.*,⁴³ (**Fig. 5c**
196 and **d**). As controls, Al-coated silicon substrates and MgAl LDH films were also probed using
197 the same cell probes. Force–distance curves were recorded during constant approach and
198 retraction of the yeast cell to the different substrates.



199
200 **Fig. 5.** SEM images of fungal probes, LDH films, and LDH-functionalized AFM tips. (a) Top view (scale
201 bar = 10 μm) and (b) side view (scale bar = 5 μm) of fungal probes prepared by attaching living *C. albicans*
202 cells (round-shaped) to tipless cantilevers coated with polydopamine (traces found on the probes). (c) MgAl

203 and (d) ZnAl LDH film grown on silicon substrates (scale bars = 2 μm). (e) MgAl-functionalized and (f)
204 ZnAl-functionalized AFM tips (scale bars = 2 μm).

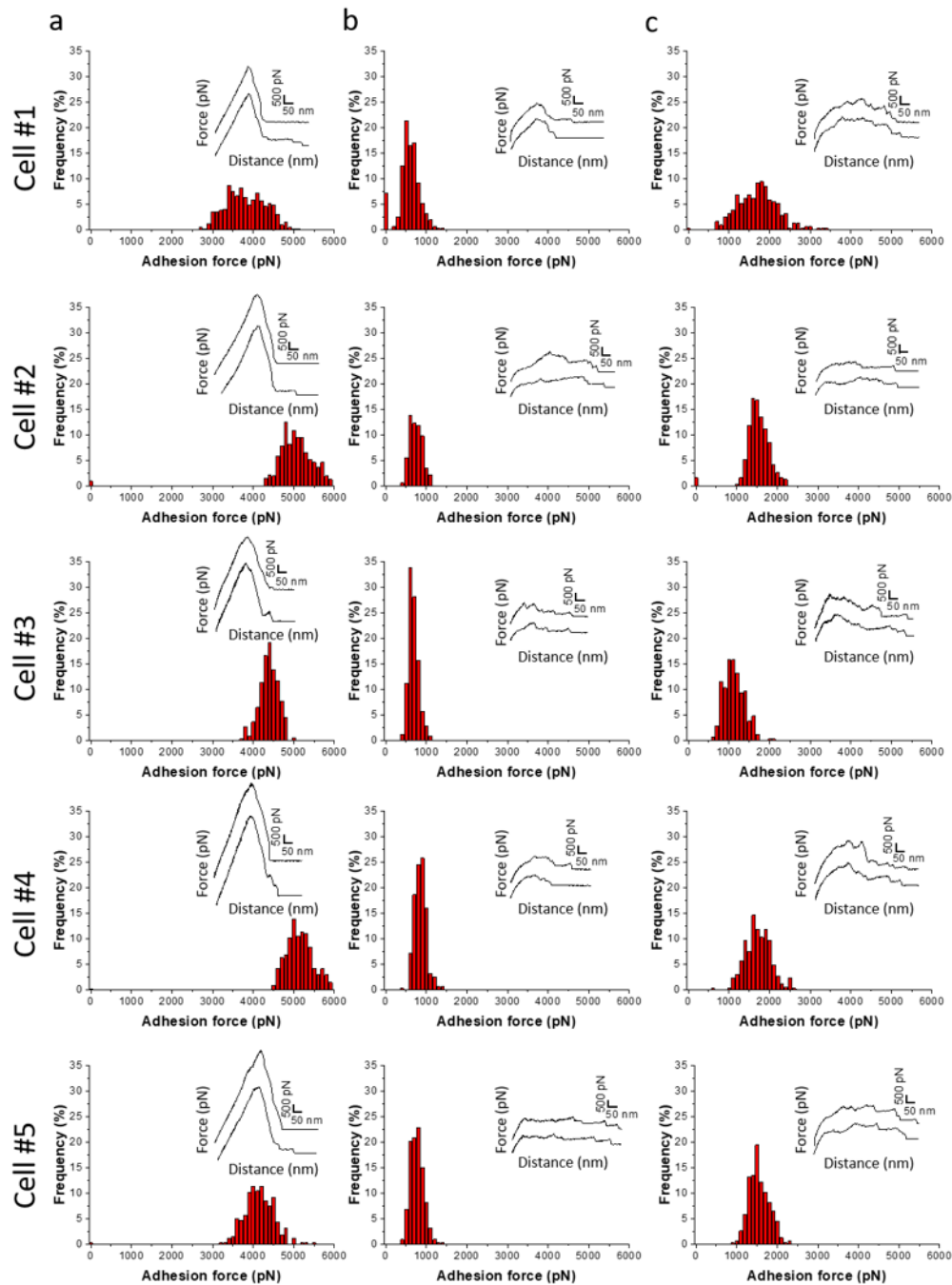
205 **Fig. 6a** shows adhesion force histograms as well as representative force-distance (FD) curves
206 obtained from probing ZnAl LDH films with different fungal probes. The adhesion frequency was
207 ~100 % as all recorded retraction FD curves showed an adhesion signature. The slight variation (<
208 2%) in adhesion frequencies among the probed ZnAl LDH film may be attributed to the
209 heterogeneity in the attached cell microarchitecture and cell wall composition. The measured
210 adhesion forces ranged from 3000 to 5000 pN with rupture lengths ranging between 140 and 650
211 nm (data not shown). Such finding suggests the presence of strong surface interactions (thousands
212 pN) occurring at the interface between the attached *C. albicans* cells and ZnAl LDH films.

213 Upon probing Al-coated silicon substrates using the same cell probes, adhesion force magnitudes
214 did not exceed 1200 pN, which represents much weaker adhesion behavior than that observed with
215 ZnAl LDH films (**Fig. 6b**).

216 MgAl LDH films probed with the same fungal probes showed slightly higher adhesion force
217 magnitudes (500-2500 pN) in comparison to Al-coated surfaces. However, their adhesion behavior
218 in terms of force magnitudes (**Fig. 6c**) was remarkably weaker than those of ZnAl LDH films.
219 Considering that MgAl and ZnAl LDH films possess similar morphologies (**Fig. 5c and d**), one
220 can deduce that the higher adhesion force magnitudes on ZnAl LDH films are not directly linked
221 to their morphology but rather to their constituent divalent metal itself, *e.g.*, Zn^{2+} , playing a major
222 role on the previously observed antifungal effect of Zn-based LDHs.¹³

223 Adhesion interactions between *C. albicans* cells and ZnAl LDHs were further probed at the single
224 LDH particle level using SPFS. For this purpose, AFM tips were functionalized with ZnAl and
225 MgAl LDH films in a similar procedure to that of the synthesis of LDH (**Fig. 5d and e**).¹⁴ Living

226 *C. albicans* cells were immobilized in porous membranes and further probed using different
227 functionalized tips, *e.g.*, ZnAl-, MgAl- and Al-functionalized AFM tips. Due to their very small
228 size, the characterizations on ZnAl- and MgAl-functionalized tips were performed on LDH films
229 grown on silicon wafers using the exact same protocol used to synthesize LDH-functionalized tips.
230 The detailed characterizations of these films are reported in our previous work.¹⁴ It is important
231 here to mention that the morphology and the thickness of ZnAl and MgAl LDH films were very
232 similar. The thickness values by SEM-cross sectional imaging were 312 ± 24 nm and 315 ± 25 nm
233 for MgAl LDH films and ZnAl LDH films, respectively. Moreover, scratch method was also used
234 to determine the thickness of the obtained films by AFM imaging and the obtained values ($314 \pm$
235 10 nm and 316 ± 12 nm for MgAl film and ZnAl LDH films, respectively) were in good agreement
236 with those found by SEM imaging.¹⁴



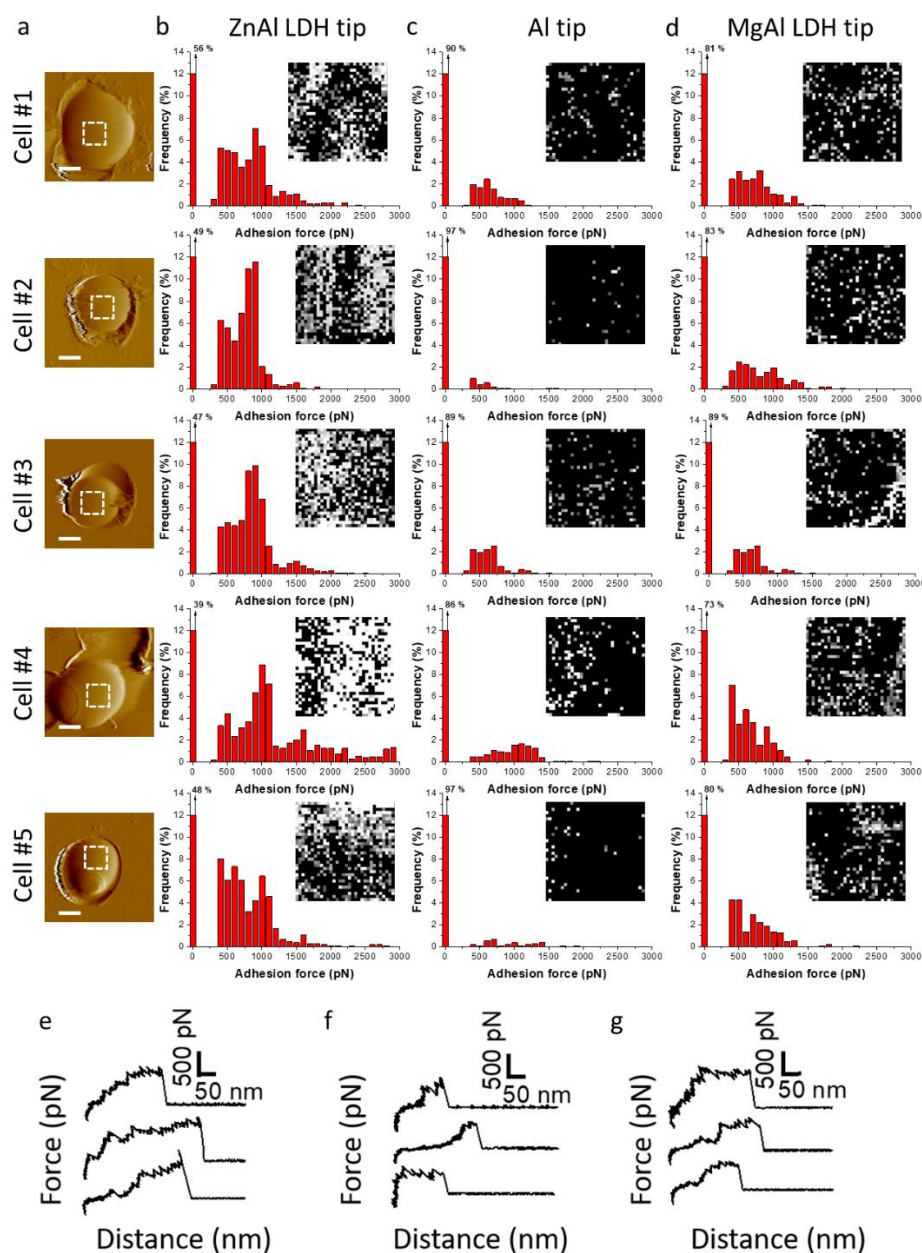
237

238 **Fig. 6.** SCFS deciphers the adhesion forces between *C. albicans* cells and LDH films at the single-cell level.
 239 (a,b,c) Adhesion force histograms obtained by recording multiple force-distance curves ($n > 1024$) between
 240 *C. albicans* cells and ZnAl LDH (a), Al (b) and MgAl LDH (c) films. Insets correspond to representative
 241 force signatures. Data were obtained from three independent experiments using different cell probes,
 242 independent cell cultures and films.

243 **Fig. 7b** and **e** show adhesion force histograms associated with adhesion force maps and
244 representative FD curves, respectively, obtained from different *C. albicans* cells probed with ZnAl
245 tips. Adhesive white-grey pixels were randomly distributed on the maps suggesting the
246 homogeneous adhesion of ZnAl LDH to the fungal cell surface. Most recorded FD curves showed
247 an adhesion signature with a frequency ranging from 44 to 61% (**Fig. 7b**). Adhesion curves showed
248 strong interactions (**Fig. 7e**), with multiple large force peaks (300-3000 pN, **Fig. 7b**) and long
249 ruptures ranging from 200 to 500 nm (data not shown). These sawtooth force signatures are
250 characteristics of Als proteins sequential unfolding in *C. albicans* cell wall.^{21,38,44,45}

251 Upon probing the same cells (**Fig. 7c**) using Al-functionalized tips, no considerable adhesion
252 between aluminum and *C. albicans* was noticed, where the adhesion frequency did not exceed
253 14%. Additionally, most rupture lengths lied below 200 nm with force magnitudes not exceeding
254 1200 pN. These few adhesive events are considered as weak non-specific interactions (FD curves
255 did not show sawtooth sequential unfolding, **Fig. 7f**) as compared to signatures obtained with of
256 ZnAl-functionalized tips.

257 MgAl-functionalized tips showed slightly higher adhesion frequencies (17 to 27%, **Fig. 7d**) and
258 force magnitudes (300 to 1500 pN, **Fig. 7d**) with FD curves showing slightly long sawtooth
259 sequential unfolding that we attribute to Als adhesive proteins (**Fig. 7g**). However, the interactions
260 observed for non-antifungal MgAl LDHs with *C. albicans* cells were much weaker than those
261 obtained by ZnAl-functionalized tips. Such observation comes in line with that of the results
262 obtained from SCFS (**Fig. 6**), indicating that the strong adhesive interactions obtained between
263 ZnAl LDHs and *C. albicans* cells are related to their antifungal nature. In fact, we have previously
264 observed such differences in adhesion behavior between antimicrobial ZnAl LDHs and non-
265 antimicrobial MgAl LDHs toward *S. aureus* bacterial cells.¹⁴



266

267 **Fig. 7.** SPFS with functionalized tips reveals specific interaction for ZnAl tips with living *C. albicans* cells.
 268 (a) Topography images of *C. albicans* cells trapped in porous membranes (scale bar = 1 μm, dashed squares
 269 display probed areas of the cell of 1 x 1 μm²) and probed with functionalized AFM tips. (b,c,d) Adhesion
 270 force histograms and adhesion force maps (insets, 1 x 1 μm²) obtained on the top of cells using ZnAl-
 271 functionalized AFM tips (b), Al-coated AFM tips (c) and MgAl-functionalized AFM tips (d). White/grey
 272 pixel corresponds to adhesive events and black pixels correspond to non-adhesive events (scale 0-1000 pN).
 273 Data were obtained from three independent experiments using different tips and independent cell cultures.
 274 (e,f,g) Representative force-distance curves obtained by probing the surface of *C. albicans* using ZnAl-
 275 functionalized (e), Al-coated (f) and MgAl-functionalized AFM tips (g).

276 We had previously established in this work that ZnAl LDH NPs possessed specific and efficient
277 antifungal properties in comparison to non-antifungal MgAl LDH NPs, which was validated by *C.*
278 *albicans* growth inhibition (**Fig. 3**) and imposing serious morphological damages to their cell walls
279 (**Fig. 4**). Therefore, the specific adhesion interactions observed for antifungal ZnAl LDHs which
280 may be attributed by the stretching of Als adhesive proteins provide strong evidence about the
281 contribution of surface adhesive interactions to the antifungal activity of ZnAl LDHs.

282 Indeed, some researchers had previously reported the antimicrobial activity of zinc-based LDHs
283 through direct surface interactions,^{13,20} however, none of them provided an evidence on the
284 presence of these interactions. The researchers claimed that zinc present in the LDH structure can
285 bind and then interact with the membranes of microorganisms providing damages to the cell wall
286 which could further lead to death. Zinc ions present on the surface of LDHs may bind to the
287 membranes of microorganisms, and it may then be transported by the uptake system for essential
288 metal ions to the cell where they could accumulate and exert toxic effects. Therefore, the
289 interactions translated in the form of forces measured between ZnAl LDHs and *C. albicans*
290 provided evidence on the presence of surface interaction which may present one key point in the
291 antifungal behavior of ZnAl LDHs.

292 In this context, ZnAl LDH NPs were able to specifically interact and adhere to *C. albicans* cells
293 with high adhesion frequency and great force magnitudes thus imposing serious damages to their
294 cell walls which consequently lead to an efficient antifungal effect against these yeast pathogens.

295 **3. Conclusion**

296 In the present study, the role of adhesive interactions in the antifungal activity of ZnAl LDH NPs
297 against *C. albicans* was studied. ZnAl LDH NPs exhibited an efficient antifungal effect against *C.*

298 *albicans* in comparison to non-antifungal MgAl LDH NPs, which was evidenced by greater
299 inhibition zone diameters generated in agar disc-diffusion assay and MIC determination by broth
300 microdilution tests. Additionally, serious morphological impacts including rough surfaces, surface
301 distortion, and dissociation into cell debris were imposed on *C. albicans* cells by ZnAl LDH NPs
302 treatment at MIC.

303 Moreover, AFM-based SCFS and SPFS were employed to probe the nanoscale adhesive
304 interactions between *C. albicans* cells and the prepared ZnAl LDH NPs to further correlate them
305 to the observed antifungal activity of the latter. For SCFS, living *C. albicans* cells were attached
306 to AFM tipless cantilevers and used to probe the surface of prepared ZnAl, MgAl and Al films at
307 the single-cell level. Whereas for SPFS, Al-coated and LDH-functionalized AFM tips were
308 prepared and used to probe surface adhesion interactions with the cell surface at the single LDH
309 particle level. SCFS showed that *C. albicans* cells interacted with ZnAl LDHs with much higher
310 force magnitudes than Al-coated surfaces and non-antifungal MgAl LDHs. Such strong adhesive
311 interactions were attributed to the antifungal nature of Zn-based LDHs arisen from their constituent
312 divalent metal, *e.g.*, Zn^{2+} . The comparison of the adhesion behavior of Al-coated, MgAl-
313 functionalized, and ZnAl-functionalized tips at the single-particle level further indicated the
314 presence of specific surface interactions occurring at high adhesion frequency and remarkable
315 force magnitudes between ZnAl LDHs and *C. albicans* cells which may be attributed to the
316 presence of Als adhesive proteins of the cells. Such finding suggested the presence of a strong
317 correlation between the specific ability of zinc-based LDHs to interact with and damage *C.*
318 *albicans* cell walls, thus correlating the antifungal properties of ZnAl LDHs to the nanoscale
319 adhesive forces occurring at the single-cell and single-particle levels with *C. albicans* fungal
320 pathogens.

321 **4. Experimental part**

322 **4.1. LDH NPs synthesis**

323 Nitrate-intercalated MgAl and ZnAl LDH NPs were synthesized similarly to our previous
324 work.¹⁴ Briefly, a mixture of 0.2 mol/L $M(\text{NO}_3)_2 \cdot 6\text{H}_2\text{O}$ ($M=\text{Zn}, \text{Mg}$; SIGMA-ALDRICH) and
325 0.1 mol/L $\text{Al}(\text{NO}_3)_3 \cdot 9\text{H}_2\text{O}$ (SIGMA-ALDRICH) was added quickly to a 0.15 M NaOH
326 solution (VWR Chemicals), under nitrogen atmosphere and vigorous stirring for 20 min. The
327 LDH slurry was obtained by centrifugation, washed twice, and dispersed again in decarbonated
328 water. The resultant suspension was then transferred to a stainless-steel autoclave with a Teflon
329 lining and heated for 24 h at 80 °C. LDH powders were then collected by centrifugation and
330 air drying at 80 °C.

331 **4.2. Synthesis of LDH films and LDH-functionalized AFM tips**

332 Nitrate-intercalated MgAl and ZnAl LDH films were grown on aluminum coated silicon
333 wafers using a wet-chemistry protocol, as previously described.¹⁴ Briefly, a thin layer of
334 aluminum (~10 nm) was deposited on silicon wafers previously cleaned with piranha solution
335 by plasma sputtering (Q150T S, Quorum). Aluminum-coated silicon substrates were then
336 transferred to a stainless-steel autoclave with a Teflon lining containing a solution of 50 mL
337 $M(\text{NO}_3)_2 \cdot 6\text{H}_2\text{O}$ ($M=\text{Mg}, \text{Zn}$; 2.5 mmol) and NH_4NO_3 (30 mmol, SIGMA-ALDRICH). The
338 autoclave was heated at 80 °C for 24 h. The obtained LDH films were then washed with
339 deionized water and ethanol and then dried using nitrogen flush. LDH-functionalized AFM
340 silicon nitride probes (MLCT-C Bruker corporation) were synthesized in a similar method to
341 that of LDH films grown on silicon wafers.

342 **4.3. Scanning electron microscopy imaging**

343 The morphology of LDH NPs, films, LDH-functionalized AFM tips, and cell probes was
344 examined by scanning electron microscopy (SEM) using a JEOL JSM-IT500HR, with a field
345 emission gun (FEG) and a voltage of 2 to 10 kV. The analysis was performed under high
346 vacuum, and 60 μm diaphragm aperture was settled. Secondary electron detector (SED) was
347 used for imaging.

348 **4.4. Antimicrobial activity tests**

349 The antimicrobial activity of MgAl and ZnAl LDH NPs was evaluated using agar disk disc
350 diffusion and broth microdilution turbidity methods against the fungal pathogen *C. albicans*
351 (SC5314).

352 Inhibition zone diameters generated by MgAl and ZnAl LDH powders were determined by agar
353 disk diffusion test. *C. albicans* cells were precultured in 5 mL sterile yeast extract peptone dextrose
354 (YPD, SIGMA ALDRICH) overnight at 30°C and then diluted to 1/1500 in sterile 3-(N-
355 morpholino)propane sulfonic acid (MOPS, Sigma). Then, 250 μL of diluted fungal suspension
356 was spread on sterilized YPD agar Petri dishes using sterile cotton-tipped swabs (COPAN) to
357 prepare a homogeneous fungal layer. Filter disks (diameter = 6mm, Dominique Dutscher) were
358 placed on the dishes and 20 μL of LDH dispersions (10 mg/mL) were loaded on the respective
359 disks. Petri dishes were then incubated at 30°C for 24 h. Afterward, inhibition zones were observed
360 around the disks. The diameters of the circular zones were measured using a centimeter ruler and
361 the mean values of three repeated trials were recorded and represented in millimeters.

362 The minimum inhibitory concentration (MIC) of LDH NPs was evaluated using the broth
363 microdilution turbidimetric method. *C. albicans* cells were precultured in 5 mL YPD overnight at
364 30°C. An inoculum of *C. albicans* was then prepared and diluted to obtain an optical density of

365 0.1 at $\lambda = 600$ nm ($OD_{600} = 0.1$). MgAl and ZnAl LDH NPs were dispersed in YPD broth, and two-
366 fold dilution series were then prepared in a 96-well microtiter plate. Each well included 25 μ L of
367 diluted LDH powder and 175 μ L of yeast inoculum. Un-inoculated broth wells containing the
368 different used LDH dispersion concentrations were used as a negative standard growth control. As
369 a positive control, 12 wells were prepared with 175 μ L yeast inoculum, and 25 μ L YPD. The
370 micro-titer plate was then sealed with parafilm and incubated at 30°C under agitation for 24 h. The
371 MIC value was recognized as the lowest concentration that had no visible turbidity due to *C.*
372 *albicans* growth.

373 **4.5. Atomic force microscopy (AFM) imaging and force spectroscopy.**

374 All AFM experiments were performed at room temperature using a Bioscope Resolve AFM
375 (Bruker corporation, Santa Barbara, CA), and the spring constants of the used cantilevers were
376 determined using the thermal noise method.⁴⁶

377 For topography images on *C. albicans*, cells were cultivated alone (untreated) or with (treated at
378 MIC) ZnAl and MgAl LDH NPs for 24 h in YPD at 30°C. *C. albicans* cells were then centrifuged,
379 washed twice in MOPS, and filtered into porous polycarbonate membranes (pore size = 3 μ m,
380 Millipore). After filtration and rough rinsing, a 1 x 1 cm² piece of the membrane was cut and
381 attached using a double-sided adhesive tape at the bottom of a Petri dish and immersed in MOPS.
382 The roughness parameter Rq (root mean square of the heights) of the cells (6 cells for each
383 condition, *e.g.*, untreated cells, ZnAl LDH NPs and MgAl LDH NPs-treated cells) was calculated
384 using the commercial Nanoscope analysis (Bruker) from AFM images performed on the top of
385 bacteria at a high magnification of 1 × 1 μ m² scanning areas (512 samples/line; 262,144 data
386 points). AFM images were acquired in peak-force tapping mode using SNL-C tips.

387 For force measurements on cells using AFM-based single-cell force spectroscopy, yeast cell
388 probes were prepared using triangular-shaped tipless cantilevers (NP-O10, Microlevers, Bruker
389 Corporation) coated with polydopamine wet adhesives. The cantilevers were immersed for 1 h in
390 a 10 mmol/L Tris buffer solution (pH = 8.5) containing 4 mg/mL dopamine hydrochloride (99%,
391 Sigma), and dried with N₂ flow. Single yeast cells deposited on a Petri dish were then attached to
392 the polydopamine-coated cantilevers by bringing the cantilever into contact with an isolated cell
393 for 1 min. Proper attachment and positioning of yeast cells on the cantilever was achieved using a
394 Bioscope Resolve (Bruker Corporation, Santa Barbara, CA) equipped with a Leica inverted
395 microscope. When the proper attachment of the yeast cell was achieved, the probe was positioned
396 over the Al, MgAl and ZnAl LDH films. Multiple force–distance curves were recorded across 5
397 mm x 5 mm areas of the films using a maximum applied force of 500 pN, an interaction time of
398 0.1 s, and constant approach and retraction speeds of 1 μm/s. Adhesion force histograms were
399 obtained by calculating for each force curve the maximum adhesion peak. Data was processed
400 using the commercial Nanoscope analysis (Bruker) and MATLAB (The MathWorks, Natick, MA)
401 softwares.

402 For force measurements on cells using AFM-based single-particle force spectroscopy, stationary
403 phase cultures of *C. albicans* were trapped in porous membranes in a similar procedure used for
404 cells imaging in MOPS. First, bare MLCT-C tips were used to localize and image individual cells.
405 Then, the tips were replaced by aluminum-coated tips, MgAl, and ZnAl LDH-functionalized tips.
406 Adhesion force maps and histograms were obtained by recording 32 × 32 force–distance curves
407 on areas of 1 x 1 μm² on cell surfaces, calculating the adhesion force of the last adhesion peak for
408 each force curve, and displaying the value as a grey pixel. All curves were recorded using a
409 maximum applied force of 500 pN, a contact time of 0.1 s, and constant approach and retraction

410 speeds of 1 $\mu\text{m/s}$. Data were processed using the commercial Nanoscope analysis (Bruker) and
411 MATLAB (The MathWorks, Natick, MA) softwares.

412 **Acknowledgments**

413 We would like to acknowledge the spectroscopy and microscopy Service Facility of SMI LCPME
414 (Université de Lorraine-CNRS– <http://www.lcpme.ul.cnrs.fr>).

415 Jazia Awassa acknowledges the French Ministry of Higher Education for her Ph.D. grant.

416 **Funding**

417 Financial support was received from the French Ministry of Higher Education (MESR), and the
418 French National Scientific Centre (CNRS).

419 **References**

- 420 1. F. Bongomin, S. Gago, R. Oladele and D. Denning, *JoF*, 2017, **3**, 57.
- 421 2. G. D. Brown, D. W. Denning, N. A. R. Gow, S. M. Levitz, M. G. Netea and T. C. White, *Sci.*
422 *Transl. Med.*, DOI:10.1126/scitranslmed.3004404.
- 423 3. M. C. Fisher, A. Alastruey-Izquierdo, J. Berman, T. Bicanic, E. M. Bignell, P. Bowyer, M.
424 Bromley, R. Brüggemann, G. Garber, O. A. Cornely, Sarah. J. Gurr, T. S. Harrison, E. Kuijper,
425 J. Rhodes, D. C. Sheppard, A. Warris, P. L. White, J. Xu, B. Zwaan and P. E. Verweij, *Nat Rev*
426 *Microbiol*, 2022, **20**, 557–571.
- 427 4. N. Robbins, T. Caplan and L. E. Cowen, *Annu. Rev. Microbiol.*, 2017, **71**, 753–775.
- 428 5. S. Costa-de-Oliveira and A. G. Rodrigues, *Microorganisms*, 2020, **8**, 154.
- 429 6. N. Wiederhold, *IDR*, 2017, **Volume 10**, 249–259.
- 430 7. N. M. Packter, *Biochemical Education*, 1995, **23**, 115.
- 431 8. D. W. Denning, *CLIN INFECT DIS*, 1998, **26**, 781–803.
- 432 9. J.-L. Xu, Y.-X. Luo, S.-H. Yuan, L.-W. Li and N.-N. Liu, *Innovations in Digital Health,*
433 *Diagnostics, and Biomarkers*, 2021, **1**, 3–7.
- 434 10. A. Vaccari, *Applied Clay Science*, 2002, **22**, 75–76.
- 435 11. M. Bini and F. Monteforte, *JAPLR*, , DOI:10.15406/japlr.2018.07.00206.
- 436 12. F. L. Theiss, G. A. Ayoko and R. L. Frost, *Applied Surface Science*, 2016, **383**, 200–213.
- 437 13. S. A. A. Moaty, A. A. Farghali and R. Khaled, *Materials Science and Engineering: C*, 2016,
438 **68**, 184–193.
- 439 14. J. Awassa, S. Soulé, D. Cornu, C. Ruby and S. El-Kirat-Chatel, *Nanoscale*, 2022, **14**, 10335–
440 10348.

- 441 15. J. Awassa, D. Cornu, S. Soulé, C. Carteret, C. Ruby and S. El-Kirat-Chatel, *Applied Clay*
442 *Science*, 2022, **216**, 106369.
- 443 16. J. Awassa, D. Cornu, C. Ruby and S. El-Kirat-Chatel, *Colloids and Surfaces B: Biointerfaces*,
444 2022, **217**, 112623.
- 445 17. S. Dutta, T. K. Jana, S. K. Halder, R. Maiti, A. Dutta, A. Kumar and K. Chatterjee,
446 *ChemistrySelect*, 2020, **5**, 6162–6171.
- 447 18. M. Li, L. Li and S. Lin, *Chinese Chemical Letters*, 2020, **31**, 1511–1515.
- 448 19. A. M. León-Vallejo, F. D. Velázquez-Herrera, Á. Sampieri, G. Landeta-Cortés and G. Fetter,
449 *Applied Clay Science*, 2019, **180**, 105194.
- 450 20. F. Peng, D. Wang, D. Zhang, H. Cao and X. Liu, *Applied Clay Science*, 2018, **165**, 179–187.
- 451 21. S. El-Kirat-Chatel and Y. F. Dufrêne, *Nanoscale Horiz.*, 2016, **1**, 69–74.
- 452 22. M. Benoit, D. Gabriel, G. Gerisch and H. E. Gaub, *Nat Cell Biol*, 2000, **2**, 313–317.
- 453 23. M. Benoit and H. E. Gaub, *Cells Tissues Organs*, 2002, **172**, 174–189.
- 454 24. D. J. Müller, J. Helenius, D. Alsteens and Y. F. Dufrêne, *Nat Chem Biol*, 2009, **5**, 383–390.
- 455 25. J. Friedrichs, J. Helenius and D. J. Muller, *Nat Protoc*, 2010, **5**, 1353–1361.
- 456 26. D. Alsteens, A. Beaussart, S. Derclaye, S. El-Kirat-Chatel, H. R. Park, P. N. Lipke and Y. F.
457 Dufrêne, *Anal. Methods*, 2013, **5**, 3657.
- 458 27. A. Beaussart and S. El-Kirat-Chatel, *The Cell Surface*, 2019, **5**, 100031.
- 459 28. A. D. Russell, *Journal of Antimicrobial Chemotherapy*, 2003, **52**, 750–763.
- 460 29. E. de Souza Araújo, A. S. Pimenta, F. M. C. Feijó, R. V. O. Castro, M. Fasciotti, T. V. C.
461 Monteiro and K. M. G. de Lima, *J Appl Microbiol*, 2018, **124**, 85–96.
- 462 30. M. T. Yassin, A. A.-F. Mostafa, A. A. Al-Askar and F. O. Al-Otibi, *Crystals*, 2022, **12**, 774.
- 463 31. A. Karimiyan, H. Najafzadeh, M. Ghorbanpour and S. H. Hekmati-Moghaddam, *Zahedan J*
464 *Res Med Sci*, , DOI:10.17795/zjrms-2179.
- 465 32. M. Jalal, M. A. Ansari, S. G. Ali, H. M. Khan and S. Rehman, *Artificial Cells, Nanomedicine,*
466 *and Biotechnology*, 2018, **46**, 912–925.
- 467 33. M. Sharma and P. Prasher, in *Nanotechnology*, eds. C. Bhargava and A. Sachdeva, CRC Press,
468 1st edn., 2020, pp. 261–276.
- 469 34. G. Vimbela, S. M. Ngo, C. Frazee, L. Yang and D. A. Stout, *IJN*, 2017, **Volume 12**, 3941–
470 3965.
- 471 35. S. El-Kirat-Chatel, A. Beaussart, D. Alsteens, D. N. Jackson, P. N. Lipke and Y. F. Dufrêne,
472 *Nanoscale*, 2013, **5**, 1105–1115.
- 473 36. F. Quilès, I. Accoceberry, C. Couzigou, G. Francius, T. Noël and S. El-Kirat-Chatel,
474 *Nanoscale*, 2017, **9**, 13731–13738.
- 475 37. M. A. Hussain, D. Ahmed, A. Anwar, S. Perveen, S. Ahmed, I. Anis, M. R. Shah and N. A.
476 Khan, *Int Microbiol*, 2019, **22**, 239–246.
- 477 38. C. Formosa, M. Schiavone, H. Martin-Yken, J. M. François, R. E. Duval and E. Dague,
478 *Antimicrob Agents Chemother*, 2013, **57**, 3498–3506.
- 479 39. M. J. Fiołka, S. Mieszawska, P. Czaplewska, A. Szymańska, K. Stępnik, W. Sofińska-Chmiel,
480 T. Buchwald and K. Lewtak, *Sci Rep*, 2020, **10**, 16352.
- 481 40. T. Sultan and S. A. Ali, *Journal of Receptors and Signal Transduction*, 2011, **31**, 39–44.
- 482 41. A. Beaussart, S. El-Kirat-Chatel, R. M. A. Sullan, D. Alsteens, P. Herman, S. Derclaye and Y.
483 F. Dufrêne, *Nat Protoc*, 2014, **9**, 1049–1055.
- 484 42. M. Laviale, A. Beaussart, J. Allen, F. Quilès and S. El-Kirat-Chatel, *ACS Appl. Mater.*
485 *Interfaces*, 2019, **11**, 48574–48582.

- 486 43. F. Zhang, L. Zhao, H. Chen, S. Xu, D. G. Evans and X. Duan, *Angew. Chem. Int. Ed.*, 2008,
487 47, 2466–2469.
- 488 44. A. Beaussart, P. Herman, S. El-Kirat-Chatel, P. N. Lipke, S. Kucharíková, P. Van Dijck and
489 Y. F. Dufrêne, *Nanoscale*, 2013, 5, 10894.
- 490 45. A. Beaussart, D. Alsteens, S. El-Kirat-Chatel, P. N. Lipke, S. Kucharíková, P. Van Dijck and
491 Y. F. Dufrêne, *ACS Nano*, 2012, 6, 10950–10964.
- 492 46. J. L. Hutter and J. Bechhoefer, *Review of Scientific Instruments*, 1993, 64, 1868–1873.
493